

# Finite Alphabet Fast List Decoders for Polar Codes

Syed Aizaz Ali Shah and Gerhard Bauch

*Institute of Communications, Hamburg University of Technology, Hamburg, Germany*  
{aizaz.shah; bauch}@tuhh.de

**Abstract**—The so-called fast polar decoding schedules are meant to improve the decoding speed of the sequential-natured successive cancellation list decoders. The decoding speedup is achieved by replacing various parts of the serial decoding process with efficient special-purpose decoder nodes. This work incorporates the fast decoding schedules for polar codes into their quantized finite alphabet decoding. In a finite alphabet successive cancellation list decoder, the log-likelihood ratio computations are replaced with lookup operations on low-resolution integer messages. The lookup tables are designed using the information bottleneck method. It is shown that the finite alphabet decoders can also leverage the special decoder nodes found in the literature. Besides their inherent decoding speed improvement, the use of these special decoder nodes drastically reduces the number of lookup tables required to perform the finite alphabet decoding. In order to perform quantized decoding using lookup operations, the proposed decoders require up to 93% less unique lookup tables as compared to the ones that use the conventional successive cancellation schedule. Moreover, the proposed decoders exhibit negligible loss in error correction performance without necessitating alterations to the lookup table design process.

## I. INTRODUCTION

Besides error correction, decoding speed is also an important factor in error control. The sequential nature of the successive cancellation (SC) [1] decoding hampers the decoding speed of polar codes. In order to tackle this issue, ways to make the SC decoding faster have been discovered besides exploring other decoding schemes, e.g., belief propagation. In that regard, various steps in the SC schedule have been identified where a block of bits is decoded in one shot using an efficient constituent decoder node instead of the serial decoding. First, simplified successive cancellation (SSC) decoder was proposed where rate-0 ( $R_0$ ) and rate-1 ( $R_1$ ) constituent decoders were exploited [2]. Later, repetition ( $Rep$ ) and single parity check ( $SPC$ ) constituent decoders were utilized in SC decoding to achieve faster decoding [3]. The use of  $R_0$ ,  $R_1$ ,  $Rep$  and  $SPC$  nodes was also extended to successive cancellation list (SCL) [4]–[6]. Other special constituent nodes and their decoding can be found in the literature, e.g., [3], [7]–[9]. An SC or SCL decoder that exploits such special nodes is referred to as a *fast* decoder. Here, the term fast successive cancellation (FSC) decoder is used for a decoder that makes use of  $R_0$ ,  $R_1$ ,  $Rep$  and  $SPC$  nodes.

The resolution of the reliability messages exchanged in the decoding process plays a significant role in the efficient hardware implementation of an SCL decoder. Ideally, a small bit-width with acceptable degradation in the error correction performance of the decoder is used. One way to navigate this trade-off is the finite alphabet decoding paradigm where  $w$ -bit integer-valued messages communicate reliability information.

In [10]–[12], the information bottleneck (IB) method was used to design finite alphabet SC and SCL decoders where the decoding operations are realized as mutual information maximizing lookup tables (LUTs). Two types of LUTs are used decoding an  $N$ -bit codeword:  $2N-2$  decoding tables that replace the log-likelihood ratio (LLR) computations with lookup operations of integers.  $N$  translation tables that translate the integer-valued messages into LLRs for path metric updates in the list decoding. It was shown that a 64-bit SCL decoder outperforms a 4-bit quantized IB SCL decoder by only a small margin [13].

The use of LUTs designed with the IB method was recently combined with the SSC decoding in [14]. This work extends the use of mutual information maximizing LUTs to FSC list decoding. It is shown that the LUTs designed for SC schedule [10], [13] are readily usable with the FSC schedule where efficient decoders for the special nodes from the literature [6] are used. Moreover, the proposed finite alphabet decoders require a considerably smaller number of decoding and translation tables. The fast decoding schedule has negligible effect on the error correction performance of an LUTs-based SCL decoder.

## II. POLAR CODES REVIEW

### A. Polar Codes

A polar code with length  $N = 2^n$ , where  $n = 1, 2, \dots$ , is described by its  $N \times N$  generator matrix  $\mathbf{F}^{\otimes n}$  where  $\otimes n$  represents the  $n$ th Kronecker product with  $\mathbf{F}^{\otimes 1} = \mathbf{F} = \begin{bmatrix} 1 & 1 \\ 0 & 1 \end{bmatrix}$  [1]. For a code rate of  $R=K/N$ ,  $N-K$  bits in  $\mathbf{u} = [u_0, \dots, u_{N-1}]^T$  are set to 0 in this work, and referred to as the *frozen* bits. The values and locations of the frozen bits are known to the decoder. The remaining  $K$  positions in  $\mathbf{u}$ , specified in the *information* set  $\mathcal{A}$ , carry the information bits. The encoding follows as  $\mathbf{x} = \mathbf{F}^{\otimes n} \mathbf{u}$ .

A polar code can be represented as a graph like that of Fig. 1 for  $N=8$ , where  $\oplus$  represents modulo-2 addition (XOR). For encoding with a given  $\mathcal{A}$ , a codeword  $\mathbf{x}$  is generated by propagating the frozen and information bits in  $\mathbf{u}$  through the graph from left to right. In the figure, a single use of the matrix  $\mathbf{F}$  is highlighted in red. The structure of a polar code is composed of a recursive application of the building block  $\mathbf{F}$ , arranged in  $n$  layers marked by the color of the dashed rectangles. The edges on any layer in the structure are enumerated as  $i=0, 1, \dots, N-1$  from top to bottom. The layers are labeled  $d = 1, \dots, n$ .

### B. Successive Cancellation (List) Decoding

The SC [1] decoder estimates  $\mathbf{u}$  bit-by-bit in a sequential manner. In the Fig. 1 representation, the LLRs propagate from

arXiv:2406.14237v1 [cs.IT] 20 Jun 2024

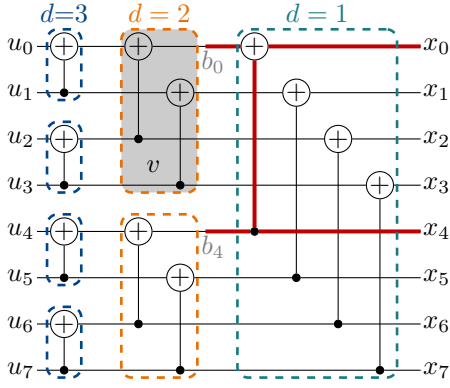


Fig. 1. Graph representation of a polar code with  $N = 8$ .

right to left and produce the decision level LLR  $L_{u_i}$  which is used to estimate  $\hat{u}_i$  for  $i \in \mathcal{A}$  as:

$$\hat{u}_i = h(L_{u_i}) = \begin{cases} 0 & L_{u_i} \geq 0 \\ 1 & \text{otherwise,} \end{cases} \quad (1)$$

where  $h(a) = \frac{1}{2}(1 - \text{sgn}(a))$  denotes hard decision decoding with  $\text{sgn}(a)$  producing  $-1$  when  $a < 0$  and  $+1$  otherwise. For  $i \notin \mathcal{A}$ , the frozen bit value is known to the decoder.

The SC decoding can also be represented by a binary decoding tree [2] like Fig. 2a. In this representation, all the decoding operations that can be performed in parallel, i.e., the dashed rectangles in Fig. 1, are condensed into a single decoder node. The leaf nodes correspond to the encoder input  $\mathbf{u}$  with frozen and information bits denoted by white and black color, respectively. Moreover, the layer label  $d$  can be interpreted as depth in the tree.

The decoding schedule activates the decoder nodes in top to bottom and left to right order. Upon activation, an *SC* node  $v$  receives  $N_v$  LLRs  $\alpha_v = [\alpha_{v,0}, \alpha_{v,1}, \dots, \alpha_{v,N_v-1}]^T$  from its parent node and is responsible for providing  $\beta_v = [\beta_{v,0}, \beta_{v,1}, \dots, \beta_{v,N_v-1}]^T$ , a bit-valued vector, to its parent node. It computes  $N_v/2$  LLRs for its left child as [15]:

$$\alpha_{l,i'} = \alpha_{v,i'} \boxplus \alpha_{v,i'+N_v/2}, \quad (2)$$

with  $0 \leq i' < N_v/2$ , and activates its left child. The boxplus operation of (2) can be approximated as:

$$\alpha_{l,i'} = \text{sgn}(\alpha_{v,i'} \alpha_{v,i'+N_v/2}) \min(|\alpha_{v,i'}|, |\alpha_{v,i'+N_v/2}|). \quad (3)$$

The node then waits for the left child to produce its decoding output  $\beta_l$ . Once  $\beta_l$  is available, the node  $v$  activates its right child by sending it the LLR vector  $\alpha_r$ , obtained as:

$$\alpha_{r,i'} = (-1)^{\beta_{l,i'}} \alpha_{v,i'} + \alpha_{v,i'+N_v/2}. \quad (4)$$

With the output of the right child  $\beta_r$  at hand, node  $v$  computes its decoding output  $\beta_v$  as:

$$\beta_{v,i} = \begin{cases} \beta_{l,i} \oplus \beta_{r,i} & \text{if } i < N_v/2 \\ \beta_{r,i-N_v/2} & \text{otherwise.} \end{cases} \quad (5)$$

If a leaf node is activated,  $\alpha_v = L_{u_i}$  and  $\beta_j = \hat{u}_j$  with the help of (1). For the root node,  $\alpha_v$  are the channel LLRs while  $\beta_v = \hat{\mathbf{x}}$ ,

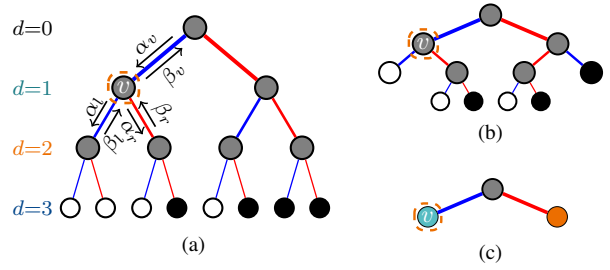


Fig. 2. Decoder-tree representations of a polar code with  $N = 8$  and  $R = 1/2$  with  $\mathcal{A} = \{3, 5, 6, 7\}$ . (a) SC, (b) Simplified SC (c) Fast simplified SC. Node types:  $\bullet$  SC,  $\circ$  R0,  $\bullet$  R1,  $\bullet$  Rep,  $\bullet$  SPC.

i.e., an estimate for the transmitted codeword. For a systematic polar code, the information bits are directly retrieved from  $\hat{\mathbf{x}}$ . In the non-systematic setting of Fig. 1, the estimated encoder input can be obtained as  $\hat{\mathbf{u}} = \mathbf{F}^{\otimes n} \hat{\mathbf{x}}$ .

Contrary to the SC decoder, an SCL [16] decoder keeps track of multiple candidate outputs. Every time a leaf node with  $i \in \mathcal{A}$  is encountered, the list decoder pursues both estimates of  $\hat{u}_i = 0$  and  $\hat{u}_i = 1$ , doubling the number of candidates. At the  $i$ th leaf node, the  $j$ th candidate in the list is assigned a path penalty metric [17] according to  $\mu_{i,j} = \mu_{i-1,j} + \Delta\mu_{i,j}$  with

$$\Delta\mu_{i,j} = \log(1 + e^{-(1-2\hat{u}_{i,j})L_{u_{i,j}}}), \quad (6)$$

for  $j \in \{0, 1, \dots, N_L-1\}$  and  $\mu_{-1,j} = 0$ . If the number of candidates in the list exceeds the specified maximum list size  $N_L$ , only the  $N_L$  most likely candidates are retained and the rest are dropped from the list. The  $\Delta\mu_{i,j}$  is approximated as [17]:

$$\Delta\mu_{i,j} = (\hat{u}_{i,j} \oplus h(L_{u_{i,j}})) |L_{u_{i,j}}| \quad (7)$$

It can be seen that (7) penalizes a path where the estimate  $\hat{u}_{i,j}$  does not match the hard decision on the LLR  $L_{u_{i,j}}$ . Once the  $N_L$  candidates for  $\mathbf{u}$  are produced by the root node, the path with smallest metric is selected as the decoder output.

### C. Fast Decoding Nodes

The fast polar decoders identify and exploit special nodes in the decoder tree of a polar code. These are in fact small polar codes of size  $N_v < N$ . These nodes can produce their output  $\beta_v$  directly from their input  $\alpha_v$  without traversing the decoding tree down to leaf nodes. The number and position of frozen bits in the  $N_v$  leaf nodes rooted in a special node defines its type. This work considers the following special nodes:

- *R0* Node: When all the  $N_v$  leaf nodes rooted in a decoder node  $v$  are frozen, it is classified as a rate 0 node [2].
- *R1* Node: A decoder node is classified as a rate 1 node when all of its associated leaf nodes correspond to information bits [2].
- *Rep* Node: When all except the right-most (i.e., last) leaf nodes of  $v$  are frozen, it is classified as a rate  $1/N_v$  repetition node [3].
- *SPC* Node: A node  $v$  with only left-most (i.e., first) leaf node being frozen is identified as a rate  $(N_v - 1)/N_v$  single parity check node [3].

Figs. 2b and 2c show the SSC and FSC decoding trees for the rate 0.5 polar code of Fig. 2a, respectively. An SCL decoder that uses the FSC decoding tree is said to use FSC schedule and, henceforth, referred to as a fast successive cancellation list (FSCL) decoder.

#### D. Fast Successive Cancellation List Decoding

This section briefly revisits the decoding procedure of the special nodes under the SCL decoding [4], [6]. Except for the node size  $N_v$ , the subscript  $v$  is dropped for the sake of brevity. Assume there are  $N_L$  paths in the list when a decoder node is activated. Each path enters the node carrying a path metric  $\mu_j$  and an LLR vector  $\alpha_j$  with  $0 \leq j < N_L$ . Further,  $\Delta\mu_j = \sum_{i=0}^{N_v-1} |\beta_{i,j} - h(\alpha_{i,j})| |\alpha_{i,j}|$  [4] denotes the path metric update for the decoding candidate  $\beta_j = [\beta_{0,j}, \beta_{1,j}, \dots, \beta_{N_v-1,j}]^T$  of a special node. The node has to produce a maximum of  $N_L$  outputs  $\beta_j$  with smallest  $\mu_j + \Delta\mu_j$ . Further, the hardware-friendly approximate formulation for the path metric update is used in the following.

Each outputs  $\beta_j$  of an  $R0$  node is an all-zero vector. Under list decoding, the node does not increase the number of paths in the list but the path metric of each path is updated by

$$\Delta\mu_j = \sum_{i=0}^{N_v-1} h(\alpha_{i,j}) |\alpha_{i,j}|. \quad (8)$$

For a  $Rep$  node, valid values of  $\beta_j$  are either all-zero or all-one vector of length  $N_v$ . Therefore, each path entering a  $Rep$  node produces two forks, with metric updates:

$$\Delta\mu_j = \begin{cases} \sum_{i=0}^{N_v-1} h(\alpha_{i,j}) |\alpha_{i,j}| & \forall \beta_j = 0 \\ \sum_{i=0}^{N_v-1} |1 - h(\alpha_{i,j})| |\alpha_{i,j}| & \forall \beta_j = 1. \end{cases} \quad (9)$$

The  $R1$  and  $SPC$  nodes have  $2^{N_v}$  and  $2^{N_v-1}$  possible outputs, respectively. Both nodes obtain the path increment  $\Delta\mu_j$  in a limited number of steps by using the Most-Likely (ML) candidate for each paths entering the node, computed as

$$\beta_j^{ML} = h(\alpha_j). \quad (10)$$

Further, let  $\alpha'_j = [\alpha'_{0,j}, \dots, \alpha'_{i'_j,j}, \dots, \alpha'_{N_v-1,j}]^T$  represent the LLRs  $\alpha_j$  sorted w.r.t. reliability, i.e.,  $|\alpha_{i,j}|$ . The  $N_L$  promising candidates to be retained in the decoding list are efficiently generated as follows [6]:

An  $R1$  node starts with initializing  $\Delta\mu_j=0$  for each ML candidate entering the node. The  $R1$  decoder sifts concurrently through  $\alpha'_j$  in the order  $0 \dots i'_j \dots s_{R1}$  with  $s_{R1} = \min(N_L - 1, N_v)$ . At each position  $i'_j$ , the decoder splits the corresponding ML path  $\beta_j^{ML}$  and increments the metric update of the new fork by  $|\alpha'_{i'_j}|$ . Once the least reliable  $s_{R1}$  positions in the ML candidates are considered, no further path splitting is done and the  $R1$  decoder retains the  $N_L$  decoding paths with smallest path metrics  $\mu_j + \Delta\mu_j$  in the list.

An  $SPC$  decoder considers  $s_{SPC} = \min(N_L, N_v)$  [6] least reliable positions in  $\alpha_j$  for path splitting. Let the least reliable

LLR position, i.e.,  $i'_j = 0$  in  $\alpha'_j$ , be denoted by  $i_{j,\min}$ . First, the parity of  $j$ th path is computed as

$$\gamma_j = \bigoplus_{i=0}^{N_v-1} \beta_j^{ML}, \quad (11)$$

and its metric update is initialized to  $\gamma_j |\alpha_{i_{j,\min}}|$ . The  $SPC$  decoder then goes through the remaining  $s_{SPC} - 1$  least reliable positions in the order  $1 \dots i'_j \dots s_{SPC}$ . At each step  $i'_j$ , a fork is created from the surviving ML paths in the list with a metric update incremented by  $|\alpha'_{i'_j}| + (1 - 2\gamma_j) |\alpha_{i_{j,\min}}|$ . Once the  $N_L$  surviving paths in the list are at hand after processing the  $s_{SPC}$  positions, the least reliable bit in each surviving path  $\beta_j$  is set to preserve the even-parity as

$$\beta_{i_{j,\min}} = \bigoplus_{i \in \{0, \dots, N_v-1\} \setminus i_{j,\min}} \beta_{i,j}. \quad (12)$$

The  $R0$ ,  $R1$  and  $Rep$  nodes in an FSCL decoder preserve the error rate of the conventional SCL decoding [4]–[6]. However, the  $SPC$  decoder leads to a minute degradation except for list size  $N_L=2$  [6].

### III. FINITE ALPHABET DECODERS

Finite alphabet decoders are a family of quantized decoders that replace LLRs with  $w$ -bit integer-valued messages, say  $t$ , in order to achieve a reduced space complexity. Each message  $t$  belongs to a finite alphabet  $\mathcal{T}$  of size  $|\mathcal{T}|=2^w$  and embeds reliability information w.r.t. a certain bit  $x$ . In other words, the message  $t$  corresponds to an LLR  $L_x(t)$ . In this work, the IB [18] method is used to design finite alphabet polar decoders.

The IB framework compresses an observation  $Y=y \in \mathcal{Y}$  into a compact form  $T=t \in \mathcal{T}$  by designating a quantity of primary relevance  $X=x$ . For the decoder design,  $x$  is some bit value, i.e.,  $x \in \{0, 1\}$ . The framework offers algorithms which accept the joint distribution  $p(x, y)$  and produce a deterministic compression mapping  $p(t|y)$ . The key idea is to determine a mapping  $p(t|y)$  which maximizes the *relevant* mutual information  $I(X; T)$  with the constraint  $|\mathcal{T}| < |\mathcal{Y}|$ . The deterministic mapping  $p(t|y)$  represents the compression operation in the form of an LUT. An IB algorithm also provides the distribution  $p(x|t)$  which is used to compute the LLR  $L_x(t) = \log \frac{p(x=0|t)}{p(x=1|t)}$  associated with each  $t \in \mathcal{T}$ .

For designing finite alphabet decoders, an integer valued alphabet  $\mathcal{T} = \{0, 1, \dots, |\mathcal{T}|-1\}$  is used here. The alphabet  $\mathcal{T}$  is chosen such that it is sorted w.r.t. the underlying LLRs, i.e.,  $L_x(t=0) < L_x(t=1) < \dots < L_x(t=|\mathcal{T}|-1)$ . Moreover, the LLRs  $L_x(t)$  are forced to exhibit odd symmetry such that

$$L_x(t = |\mathcal{T}|/2 - 1 - k) = -L_x(t = |\mathcal{T}|/2 + k),$$

where  $k = 0, \dots, |\mathcal{T}|/2 - 1$ .

In the following, the design of quantized polar decoder using the IB method from [10], [11] is revisited briefly.

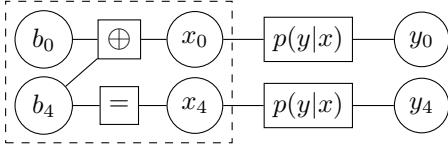


Fig. 3. Factor graph of the building block and the transmission channel.

### A. Decoder Design

The process of generating LUTs for decoding is explained using Fig. 3 on a single building block (highlighted in red color in Fig. 1). In Fig. 3,  $p(y|x)$  represents a quantized binary input AWGN channel.

First, the IB method is used to quantize the underlying AWGN channel such that  $y_i \in \mathcal{T}$  [19]. The channel quantizer provides the LLRs  $L_x(y_i)$ . With the quantized channel outputs  $\mathbf{y}=[y_0, y_4]^T$  and  $L_x(y_i)$  at hand, the IB algorithm constructs the observed LLR space using (2) for the upper branch in Fig. 3. The algorithm places  $|\mathcal{T}| - 1$  boundaries in the sorted observed LLR space and optimizes them such that  $I(B_0; T_0)$  is maximized. This results in a compression mapping  $p(t_0|\mathbf{y})$  with  $t_0 \in \mathcal{T}$ , as well as the LLRs  $L_{b_0}(t_0)$ . The LUT  $p(t_0|\mathbf{y})$  compresses the input alphabet of size  $2^{2w}$  to an output alphabet of size  $|\mathcal{T}|=2^w$ .

For the lower branch in Fig. 3, the observed LLR space is constructed from the LLRs  $L_x(y_i)$  of the quantized channel outputs  $\mathbf{y}=[y_0, y_4]^T$ , and  $\hat{b}_0 \in \{0, 1\}$  according to (4). The  $|\mathcal{T}| - 1$  boundaries in the sorted observed LLR space are optimized such that  $I(B_4; T_4)$  is maximized. The result is an LUT  $p(t_4|\mathbf{y}, \hat{b}_0)$  with  $t_4 \in \mathcal{T}$  which compresses the input alphabet of size  $2^{2w+1}$  to an output alphabet of size  $2^w$ , as well as the LLRs  $L_{b_4}(t_4)$ .

The LUTs  $p(t_0|\mathbf{y})$  and  $p(t_4|\mathbf{y}, \hat{b}_0)$  are valid for the upper and the lower branch updates, respectively, of each building block on the first layer (blue dashed rectangle) in Fig. 1. The aforementioned procedure is recursively extended to the next layers in Fig.1 to obtain compression mapping for each building block branch as detailed in [10], [11]. As a result, a total of  $2N-2$ , same as the number of edges in Fig. 2a, distinct compression mappings are obtained for a polar code of length  $N$ . The AWGN channel quantizer as well as the decoder LUTs are designed offline for a certain  $E_b/N_0$ , which is referred to as the design  $E_b/N_0$  of the finite alphabet decoder designed using the IB method.

### B. LUT based Successive Cancellation List Decoding

The decoder tree representation of Fig. 2a is used to explain the LUT-based finite alphabet decoding. Half of the  $2N-2$  mappings utilize (2) in their design and correspond to the left edges in Fig. 2a. The remaining  $N-1$  LUTs use (4) during their design and correspond to the right edges in the figure.

At the start of the finite alphabet decoding, the root node receives the integer-valued quantized channel outputs  $\alpha_v=[y_0, \dots, y_7]^T$ . The root node determines  $\alpha_l$  for its left child using the LUT  $p(t_{i'}|y_{i'}, y_{i'+N_v/2})$  with  $i'=0, \dots, N_v/2$ , i.e., the mapping  $p(t_0|\mathbf{y})$  with adjusted labels. Since the LUT

$p(t_0|\mathbf{y})$  replaces the LLR arithmetic of (2), it is referred to as a *decoding table*. The list of LLRs  $L_{b_0}(t_0)$  is referred to as the *translation table* for  $t_{i'}$  as it translates each integer-valued message into its reliability information.

When the left child produces its decoding output  $\beta_l$ , the root node computes  $\alpha_r$  for its right child using the LUT  $p(t_4|\mathbf{y}, \hat{b}_0)$  as  $p(t_{i'}|y_{i'}, y_{i'+N_v/2}, \beta_{l,i'})$  with  $i'=0, \dots, N_v/2$ . As the LUT replaces the LLR arithmetic (4), it is termed a decoding table and it comes with its own translation table, i.e., the list of LLRs  $L_{b_4}(t_4)$ . After the right child produces its decoding output  $\beta_r$ , it is combined with  $\beta_l$  according to (5).

Each node in the decoding tree uses a separate decoding table to produce integer-valued inputs for its left or right child indicated by blue or red edges, respectively, in Fig. 2a. Every leaf node is reached after using a different sequence  $n$  decoding tables (the sequence of  $n$  edges connecting the root node to the leaf node). At each leaf node, a separate translation table is used to convert the integer messages into LLRs for path metric update according to (6) or (7). Thus, although the decoder design procedure creates a translation table associated with each of the  $2N-2$  decoding tables, only  $N$  translation tables are used in the SCL decoding.

## IV. FINITE ALPHABET FAST SUCCESSIVE CANCELLATION LIST DECODING

This section explains how the LUTs generated for SC schedule in Sec. III can be used in the fast decoding schedules. The main difference arises from the use of decoding trees of Figs. 2b or 2c instead of Fig. 2a.

The fast finite alphabet decoding starts with the root node receiving the integer-valued quantized channel outputs  $y_0, \dots, y_7$ . The root node activates its children at depth  $d=1$  exactly as explained in Sec. III-B. Consider the instance when the left child marked  $v$  at  $d=1$  in Fig. 2 is activated. The node  $v$  receives  $\alpha_v=[t_0, \dots, t_3]^T$  from the root node. From  $\alpha_v$ , the node produces  $\alpha_l$  for its left child using the LUT corresponding to the edge between the two nodes. Under the SSC schedule, the left child is an  $R0$  node. The rate-0 child translates the integer-valued messages in  $\alpha_l$  to LLRs and produces its output  $\beta_l$  as explained in Sec. II-D. The right child of  $v$  is a normal node which produces its output  $\beta_r$  by traversing the tree down to the maximum depth  $d=3$ .

On the other hand, the FSC tree only has two leaf nodes that are children of the root node. Under the FSC schedule, the node  $v$  already is a special, i.e., *Rep*, node. Thus, node  $v$  translates  $\alpha_v$  into LLRs using the translation table  $L_{b_0}(t_0)$  from Sec. III-B and produces  $\beta_v$  according to the repetition node decoding of Sec. II-D. Similarly, the right child is an *SPC* node. When activated, the *SPC* node translates the integer-valued messages it receive from the root node using the translation table  $L_{b_4}(t_4)$  from Sec. III-B. The *SPC* node produces its output from the translated LLRs as described in Sec. II-D.

The number of decoding tables required by a decoder schedule depends upon the number of edges in its respective decoding tree. For the example of Fig. 2, the SC schedule

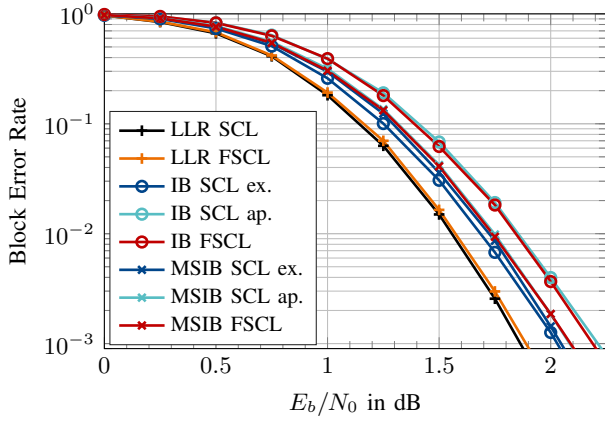


Fig. 4. Quantized SCL decoding under SC and FSC schedules.  $N=1024$ ,  $R=0.5$ ,  $N_{\text{CRC}}=16$ ,  $N_L=32$ , and BPSK over AWGN channel.

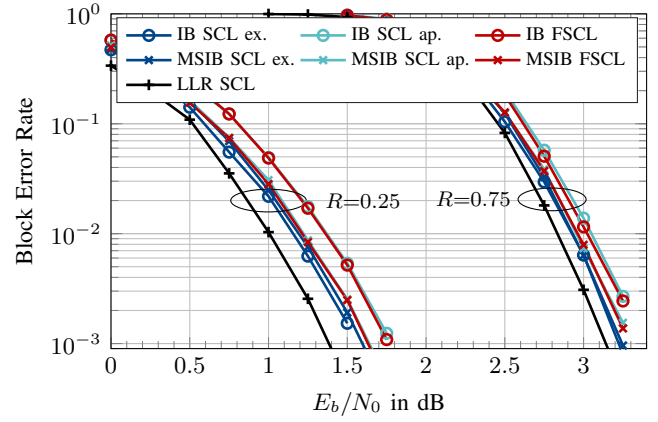


Fig. 5. Quantized SCL decoding under SC and FSC schedules.  $N=1024$ ,  $R=0.25$  and  $0.75$ ,  $N_{\text{CRC}}=16$ ,  $N_L=32$ , and BPSK over AWGN channel.

requires 14 decoding tables. On the other hand, the SSC and FSC require 10 and only 2 decoding tables, respectively.

The number of translation tables required for SCL decoding depends upon the number of leaf nodes in a schedule's decoder tree. For Fig. 2, the SC schedule requires  $N = 8$  translation tables. The SSC schedule requires 6 translation tables. The FSC schedule requires only 2 translation tables.

## V. RESULTS

This section presents simulation results for the error correction performance of the proposed LUT-based fast SCL decoders. The proposed decoder is compared at a block error rate of  $10^{-3}$  with a double-precision floating-point LLR-based SCL decoder as well as the finite alphabet decoders of [10], [13]. The LUT-based decoders of [10], recapped in Sec. III-A, are labeled as IB. The decoders from [13] which use the min-sum approximation of (3) during the decoder design instead of (2) are labeled as MSIB. The labels "ex." and "ap." indicate the use of exact and approximate path metric updates according to (6) and (7), respectively, in the SC schedule of finite alphabet decoders. The proposed decoders make use of the LLR-based constituent decoders for the special nodes in their FSC schedule. These constituent decoders use the hardware-friendly approximate path metric updates (cf. Sec. II-D).

The LUTs for both IB and MSIB decoders were generated with  $|\mathcal{T}|=16$ , i.e., 4-bit resolution. All the simulations were performed for a codeword length of  $N=1024$ , list size of  $N_L=32$  and CRC size of  $N_{\text{CRC}}=16$  over an AWGN channel using BPSK modulation. The code construction was adopted from 5G NR [20].

Fig. 4 presents block error rates for  $R=0.5$  where the LUT-based decoders were designed for  $E_b/N_0=0.5$  dB. As reported in [11], the use of approximate path metrics causes a visible degradation in the IB SCL decoding. Compared to the approx. 0.17 dB performance loss of the IB SCL decoder, the MSIB SCL decoder suffers a smaller degradation of 0.05 dB due to the path metric approximation. Further, it can be seen that the proposed IB FSCL and MSIB FSCL preserve the error correction performance of IB and MSIB decoders with approximate path metrics, respectively.

The loss due to path metric approximation can be avoided in the LUT-based decoders operating on an SC schedule: Instead of translating the messages to LLRs and subsequently updating path metrics, the translation tables are modified such that the integer-valued messages are translated to pre-computed exact metric updates [11]. A similar workaround can be tried in the proposed fast decoders. However, we restrict ourselves in this work to employing efficient constituent decoders from existing literature that exploit the approximate path metrics. Within this framework, the MSIB fast SCL decoder emerges as a favorable option. The proposed 4-bit MSIB FSCL decoder shows a degradation of 0.2 dB w.r.t. the 64-bit LLR-based FSCL decoder. Compared to the quantized SCL decoders, the speed from using the FSC schedule costs approx. 0.05 dB.

Fig. 5 provides results for code rates of 0.25 and 0.75 with the quantized decoders designed for 0.0 dB and 1.75 dB. Trends similar to Fig. 4 can be seen in Fig. 5, i.e., the proposed IB FSCL and MSIB FSCL preserving their error correction performance of SC schedule with approximate metric updates. Here too, the proposed MSIB FSCL outperforms the IB FSCL.

In LLR-based FSCL decoding, the *SPC* nodes are known to cause a slight degradation [6]. However, the proposed FSCL decoders seem to either match or very slightly outperform their SC schedule counterparts. Fig. 6 shows result of an experiment where the same codeword is decoded by a partially enabled fast schedule with only certain types of the special nodes retained in the decoder tree and replacing the rest with *SC* nodes. The labels in 6 indicate the type of nodes enabled in the FSC schedule. In the case of Fig. 6a, only one type of the nodes, i.e.,  $R_0$ ,  $R_1$ ,  $Rep$  or  $SPC$ , are enabled while multiple node types are enabled in the case of Fig. 6b. Fig. 6a shows that the *SPC* type nodes do cause slight degradation. The same suggested is by Fig. 6b when  $R_0$ ,  $R_1$  and  $Rep$  nodes are enabled but *SPC* nodes are not.

The translation of integer-valued messages into LLRs always happens at an earlier depth  $d < n$  in the FSC schedule as seen in the compact representation of FSC schedule for the rate  $R=0.5$  polar code in Fig. 7. Instead of the huge FSC decoding tree for  $N=1024$ , Fig. 7 presents the schedule as a sequence of constituent decoders from  $i_v=1$  to  $i_v=86$  together

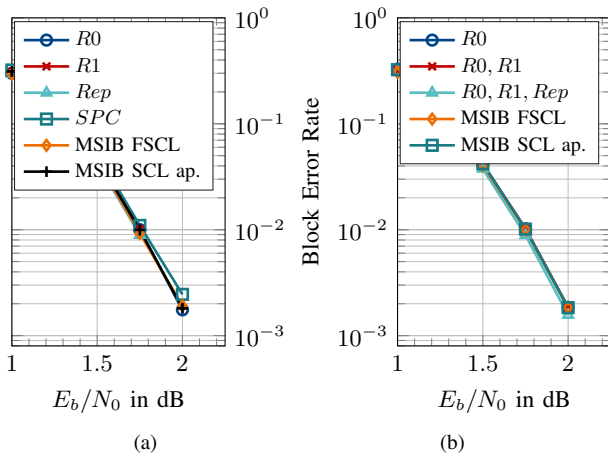


Fig. 6. Effect of special nodes in MSIB FSCL decoding.

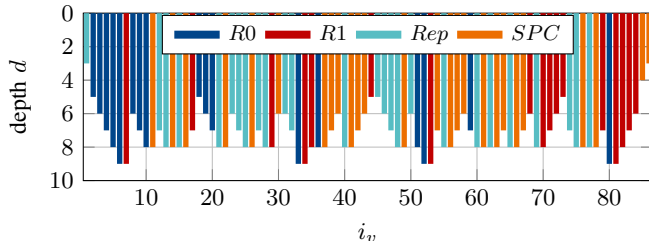


Fig. 7. Sequence of nodes and their depth  $d$  in the decoder tree under FSC schedule for  $N=1024$ ,  $K=512$  and  $N_{CRC}=16$ . i.e.,  $|\mathcal{A}| = 528$ .

with depth  $d$  of each node in the tree. The early translation of messages cuts back the loss caused by the  $SPC$  nodes as messages at depth  $d < n$  are subject to less compression by the IB framework.

Table. I presents the number of unique LUTs required by the proposed decoders for various code rates. The number of decoding tables required for LUT-based SCL decoding is equal to the number of edges in its decoder tree. The number of translation table is equal to the number of leaf nodes in the decoder tree. An IB SCL decoder requires  $2N-2=2046$  distinct decoding tables and  $N=1024$  translation tables [10] regardless of the code rate. The MSIB SCL [13] requires  $N=1024$  decoding as well as  $N$  translation tables. In comparison, the IB and MSIB FSCL decoders require as few as 71 translation tables. Depending upon the code rate, the proposed IB FSCL requires as few as 140 decoding tables instead of 2046. Similarly, the MSIB FSCL requires 71 to 86 decoding tables. These number show a remarkable reduction in the number of LUTs used for performing the proposed finite alphabet decoding, i.e., up to 93%.

## VI. CONCLUSION

In this paper, the design of LUT-based quantized polar decoders was extended to use fast decoding schedules. The fast schedules increase the decoding speed of SCL decoders by deploying special constituent decoders. It was shown that the LUTs designed for conventional SC schedule can be used for the fast SC schedule without needing any change in the design process of the LUTs. The potential increase in decoding

TABLE I  
NUMBER OF REQUIRED LOOKUP TABLES FOR PROPOSED DECODERS

table type	IB FSCL			MSIB FSCL		
	$R=0.25$	$R=0.5$	$R=0.25$	$R=0.25$	$R=0.5$	$R=0.25$
Decoding	140	170	148	71	86	75
Translation	71	86	75	71	86	75

speed of the fast SC schedules has negligible effect on the error correction performance. Most importantly, the need for distinct LUTs in the proposed finite alphabet decoders reduces by up to 93%.

## REFERENCES

- [1] E. Arikan, "Channel Polarization: A Method for Constructing Capacity-Achieving Codes for Symmetric Binary-Input Memoryless Channels," *IEEE Transactions on Information Theory*, vol. 55, no. 7, pp. 3051–3073, Jul. 2009.
- [2] A. Alamdar-Yazdi and F. R. Kschischang, "A simplified successive-cancellation decoder for polar codes," *IEEE Communications Letters*, vol. 15, no. 12, pp. 1378–1380, 2011.
- [3] G. Sarkis, P. Giard, A. Vardy, C. Thibault, and W. J. Gross, "Fast polar decoders: Algorithm and implementation," *IEEE Journal on Selected Areas in Communications*, vol. 32, no. 5, pp. 946–957, 2014.
- [4] —, "Fast list decoders for polar codes," *IEEE Journal on Selected Areas in Communications*, vol. 34, no. 2, pp. 318–328, 2016.
- [5] S. A. Hashemi, C. Condo, and W. J. Gross, "Simplified successive-cancellation list decoding of polar codes," in *2016 IEEE International Symposium on Information Theory (ISIT)*, 2016, pp. 815–819.
- [6] —, "Fast and flexible successive-cancellation list decoders for polar codes," *IEEE Transactions on Signal Processing*, vol. 65, no. 21, pp. 5756–5769, 2017.
- [7] M. Hanif and M. Ardakani, "Fast successive-cancellation decoding of polar codes: Identification and decoding of new nodes," *IEEE Communications Letters*, vol. 21, no. 11, pp. 2360–2363, 2017.
- [8] C. Condo, V. Bioglio, and I. Land, "Generalized fast decoding of polar codes," in *2018 IEEE Global Communications Conference (GLOBECOM)*, 2018, pp. 1–6.
- [9] Y. Shen, Y. Ren, A. T. Kristensen, A. Balatsoukas-Stimming, X. You, C. Zhang, and A. P. Burg, "Fast sequence repetition node-based successive cancellation list decoding for polar codes," in *ICC 2022 - IEEE International Conference on Communications*, 2022, pp. 116–122.
- [10] S. A. A. Shah, M. Stark, and G. Bauch, "Design of quantized decoders for polar codes using the information bottleneck method," in *Intl. ITG Conf. Systems, Commun., Coding (SCC)*, 2019.
- [11] —, "Coarsely Quantized Decoding and Construction of Polar Codes Using the Information Bottleneck Method," *Algorithms*, vol. 12, no. 9, p. 192, Sep. 2019.
- [12] T. Koike-Akino, Y. Wang, S. Cayci, D. S. Millar, K. Kojima, and K. Parsons, "Hardware-efficient quantized polar decoding with optimized lookup table," in *OptoElectron. and Commun. Conf. (OECC) and Int. Conf. Photon. Switching Comput. (PSC)*, 2019.
- [13] S. A. A. Shah, M. Stark, and G. Bauch, "Space-Efficient Quantized Polar Decoders Designed using the Information Bottleneck Method," in *Intl. ITG Workshop Smart Antennas (WSA) and Conf. Syst., Commun., Coding (SCC)*, 2023.
- [14] P. Giard, S. A. A. Shah, A. Balatsoukas-Stimming, M. Stark, and G. Bauch, "Unrolled and pipelined decoders based on look-up tables for polar codes," in *2023 12th International Symposium on Topics in Coding (ISTC)*, 2023, pp. 1–5.
- [15] C. Leroux, I. Tal, A. Vardy, and W. J. Gross, "Hardware architectures for successive cancellation decoding of polar codes," in *2011 IEEE International Conference on Acoustics, Speech and Signal Processing (ICASSP)*, 2011, pp. 1665–1668.
- [16] I. Tal and A. Vardy, "List Decoding of Polar Codes," *IEEE Transactions on Information Theory*, vol. 61, no. 5, pp. 2213–2226, May 2015, conference Name: IEEE Transactions on Information Theory.
- [17] A. Balatsoukas-Stimming, M. B. Parizi, and A. Burg, "LLR-Based Successive Cancellation List Decoding of Polar Codes," *IEEE Transactions on Signal Processing*, vol. 63, no. 19, pp. 5165–5179, Oct. 2015.

- [18] N. Tishby, F. C. Pereira, and W. Bialek, "The Information Bottleneck Method," in *Proceedings 37th Allerton Conference on Communication and Computation*, 1999.
- [19] J. Lewandowsky and G. Bauch, "Information-Optimum LDPC Decoders Based on the Information Bottleneck Method," *IEEE Access*, vol. 6, pp. 4054–4071, 2018.
- [20] 3<sup>rd</sup> Generation Partnership Project (3GPP), "Multiplexing and channel coding," *3GPP 38.212 V.15.3.0*, 2018.